Discrete and Continuous Dynamical Systems

doi:10.3934/dcds.2023078

CONVERGENCE OF A MOBILE DATA ASSIMILATION SCHEME FOR THE 2D NAVIER-STOKES EQUATIONS

Animikh Biswas[1], Zachary Bradshaw[*2] and Michael Jolly[3]

[1]University of Maryland Baltimore County, USA

[2]University of Arkansas, USA

[3]Indiana University, USA

(Communicated by Eduard Feireisl)

Abstract. We introduce a localized version of the nudging data assimilation algorithm for the periodic 2D Navier-Stokes equations in which observations are confined (i.e., localized) to a window that moves across the entire domain along a predetermined path at a given speed. We prove that, if the movement is fast enough, then the algorithm perfectly synchronizes with a reference solution. The analysis suggests an *informed* scheme in which the subdomain moves according to a region where the error is dominant is optimal. Numerical simulations are presented that compare the efficacy of movement that follows a regular pattern, one guided by the dominant error, and one that is random.

1. **Introduction.** Data assimilation is concerned with recovering the fine scale activity of a dynamical system via coarse measurements of that system [11, 21]. In applications, exact knowledge of an initial state is often unavailable. However, sensors often continuously monitor activity at a coarse scale. This, for instance, is the case in atmospheric sciences where, since the launch of the first weather satellites in the 1960s, weather data has been collected nearly continuously in time. These measurements provide us with partial knowledge of the state of the system, e.g., the velocity vector field or temperature, on a coarse spatial grid of points. In data assimilation, forecasting is achieved by supplementing a model with coarse measurements as opposed to a complete initial state. Many other applications exist including, but not limited to, environmental sciences, systems biology and medicine [22], imaging science, traffic control and urban planning, economics and finance and oil exploration [2].

In [3, 4], Azouni, Olson and Titi introduced a nudging based data assimilation algorithm which is mathematically rooted in earlier work on determining functionals [14, 15, 19, 20]. The concept of nudging is, however, much older and was developed to address geophysical and control problems. An upside of the approach of [3] is its ease of implementation and amenability to rigorous analysis. In contrast, for more traditional approaches to data assimilation, e.g., the Bayesian and variational frameworks, issues of stability, accuracy and catastrophic filter divergence persist

2020 *Mathematics Subject Classification.* Primary: 35Q30; Secondary: 76M22.

Key words and phrases. Data Assimilation, nudging, Navier-Stokes equations.

*Corresponding author: Zachary Bradshaw.

[18, 30, 31]. Since [3], the nudging scheme has received a great deal of attention from the fluids community. A partial list of references are [1, 5, 7, 8, 9, 12, 13, 24].

In the Azouni, Olson and Titi setup, the coarse grid on which data is collected must span the entire domain. This may be costly or unrealistic in real world settings. Therefore, it is desirable to develop a data assimilation algorithm which either does not require data to be continuously collected across the full domain or requires observations across the full domain only at a very coarse scale (in time and space). In [6] we demonstrated that, within an error, a localized, stationary collection of observations taken from an *observability region* can approximate a reference flow—i.e., synchronization occurs up to a non-zero error in contrast to [3] where synchronization is exact. A numerically visible defect of the method is that the convergence rate of global synchronization, while exponential, is slower than that of local synchronization on the observability region. The rapid local synchronization slows down global synchronization because the feedback operator is itself local (to the observability region). This means that, when the reference and approximating solutions are locally almost synchronized, the nudging becomes ineffective. If the observability window is moved to a region where the reference and approximating solutions are not locally almost synchronized, then the nudging is strengthened, at least until local synchronization occurs in the new region. This intuitive discussion suggests that building mobility into the localized nudging operator will result in improved synchronization compared to the immobile localized setup of [6]. These insights are supported by numerical work on the Navier-Stokes equations [6, 17]—see also [23]. In particular, Franz, Larios and Victor provide a detailed examination of a number of mobile paradigms, the so called "bleeps, sweeps and creeps" [17], which outperform the static observer case (with the same number of measurements) in simulations.

In the present paper, we rigorously show that a certain mobile data assimilation scheme *exactly synchronizes* with a reference solution provided the observers are moving fast enough. We additionally study features of mobile data assimilation numerically. Our numerical findings are: 1. increasing the frequency at which an observability window moves across the domain leads to faster convergence and 2. choosing the observability window based on an even coarser decision protocol improves convergence compared to a pre-determined movement pattern. We shall refer to this as the informed scheme. The main motivations for local data assimilation are that fine-scale measurements may be more expensive to obtain and that collecting fine-scale data may be infeasible in parts of the domain (e.g., in the upper atmosphere or deep in the ocean). In our numerical implementation, the dominant region is identified by coarse-scale measurements only. Thus, the dominant scheme provides the possibility that one may not have to collect fine-scale data from such regions if they remain *inactive* until global synchronization has occurred at a high level of accuracy.

In our simulations, we found that the dominant scheme synchronizes faster than schemes where the subdomain moves in a regular pattern or moves randomly. In some cases the motion of the observability window is discontinuous. Physically, this discontinuous movement is consistent with the deployment of different sets of observers consecutively in different regions as chosen by a decision protocol. A contrived example where discontinuous motion makes sense in weather forecasting is as follows: If the protocol says observations should first be taken over California and, later, over New York, then drones stationed in California could first be deployed

and, later, drones from New York could be used. To be realistic, we also simulate the effect of delay in moving the observation domain.

1.1. **Notation and preliminaries.** We consider the two-dimensional Navier-Stokes equations (henceforth, 2D NSE) on $\Omega = [-L/2, L/2]^2$ with periodic boundary conditions. For $U \subset \Omega$, we use $L^p(U)$ and $H^s(U)$ to denote the Lebesgue spaces and L^2 based Sobolev spaces respectively. If U is omitted it is understood that $U = \Omega$. We use $\langle \cdot, \cdot \rangle$ to denote the L^2 inner product. The Leray projection of L^2 onto mean zero divergence free functions in L^2 is denoted by $\mathbb{P}$. Note that for periodic boundary conditions, $\mathbb{P}\Delta = \Delta\mathbb{P}$ and we therefore do not need to introduce the Stokes operator, cf. [3, p. 284]. We use $|\cdot|$ to denote the absolute value of a vector or scalar and the 1D or 2D Lebesgue measure of a measurable set—the meaning will always be clear based on context. The characteristic function for the set S is denoted χ_S.

We make frequent use of the Poincaré and Ladyzhenskaya inequalities which respectively say: For $u \in H^1(\Omega)$,

$$\|u\|_{L^2} \leq \lambda_1^{-1/2} \|\nabla u\|_{L^2} \text{ and } \|u\|_{L^4} \leq C_L \|u\|_{L^2}^{1/2} \|\nabla u\|_{L^2}^{1/2}. \tag{1}$$

The prefactors can be viewed as the optimal constants for which these estimates hold (λ_1 is the first eigenvalue of the Laplace operator).

Data assimilation in the spirit of [3] uses an interpolant operator to nudge an assimilating solution toward a reference flow. In the present paper, this will be based on a "type 1" interpolant I_h defined using volume elements:

$$I_h f(x) = \sum_{i=1}^{M^2} \left(\chi_{S_i}(x) - \frac{h^2}{L^2} \right) \frac{1}{h^2} \int_{S_i} f \, dy,$$

where the periodic domain Ω has been split into M^2 identical squares S_i with disjoint boundaries and side lengths h. The second term in the difference ensures this operator is mean zero. It is bounded in L^2 and satisfies a Poincaré-type inequality [3]

$$\|u - I_h(u)\|_{L^2} \leq Ch \|\nabla u\|_{L^2}. \tag{2}$$

These considerations are independent of periodicity and apply in any square domain. Project onto low Fourier modes is another example of a type 1 interpolant. However, it requires global knowledge of a flow and therefore is inappropriate for out application.

1.2. **The mobile framework.** We now adapt the operator I_h to our mobile setting. Fix $N \in \mathbb{N} \setminus \{1\}$. We split Ω into a grid of N^2 squares where N is chosen to equal $2^{\tilde{N}}$ for some $\tilde{N}$—in other words the side length of our partition is taken from a dyadic scale. Each square will correspond to an observability region. We label these sub-regions Ω_i, $i = 1, \ldots, N^2$. Note that $|\Omega_i| = \frac{L^2}{N^2}$. Let $\ell = \sqrt{|\Omega_i|} = L/N$. Let $x^i = (x_1^i, x_2^i)$ be the center of Ω_i. Each Ω_i represents an "observability region," i.e. the domain from which data will be collected at a given time. Note that this partition does *not* correspond to the fine grid on which we will make observations, namely that corresponding to the length scale h in the definition of I_h above.

We work with a partition of unity $\{\phi_i\}_{i=1}^{N^2}$ of Ω so that each ϕ_i localizes to Ω_i. The functions ϕ_i are chosen to satisfy the following properties (which are illustrated in Figure 1 below):

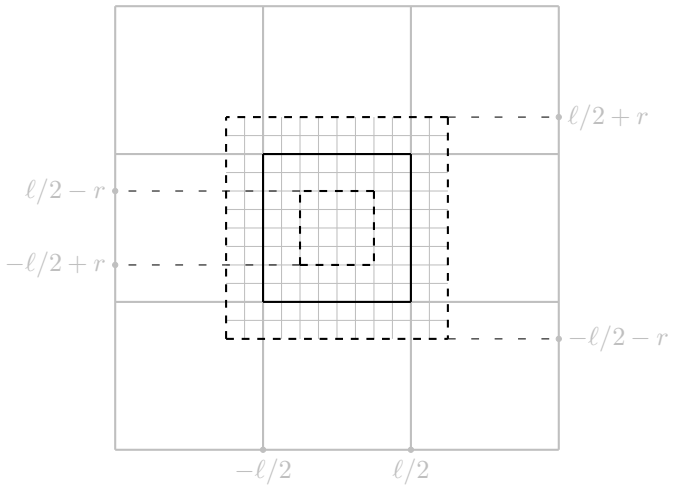

FIGURE 1. An illustration of Ω_i, which is represented by the solid black square, and adjacent cells. Ω_i is taken to be centered at the origin. The larger dashed square represents $\tilde{\Omega}_i$. The cut-off function ϕ_i is identically 1 inside the smaller dashed square and is supported inside $\tilde{\Omega}_i$. When $\iota(t) = i$, the interpolant $I_{h,t}$ is using observations taken on the fine-scale gray grid; note that observations spill over into a small region outside of Ω_i. The lengths of all squares in view are taken along a dyadic scale.

- Each ϕ_i is generated by translating ϕ_1.
- There exists $r < \ell/2$ so that $\phi_1 \equiv 1$ on $[x_1^1 - \ell/2 + r, x_1^1 + \ell/2 - r] \times [x_2^1 - \ell/2 + r, x_2^1 + \ell/2 - r]$.
- $\operatorname{supp} \phi_1 \subset \tilde{\Omega}_i := [x_1^1 - \ell/2 - r, x_1^1 + \ell/2 + r] \times [x_2^1 - \ell/2 - r, x_2^1 + \ell/2 + r]$.
- $0 \le \phi_1 \le 1$.
- $\sum_i \phi_i = 1$.
- We have
$$|\nabla \phi_1| \lesssim_{\phi_1} r^{-1} \text{ and } |\Delta \phi_1| \lesssim_{\phi_1} r^{-2},$$
where the suppressed constants only depend on the function ϕ_1.

Note the definition of $\tilde{\Omega}_i$ above as this plays an important role. We fix $r = \ell/4$ to ensure the boundaries of $\tilde{\Omega}_i$ line up with dyadic partitions at finer scales.

We quickly construct a partition of unity of this form. Let η be a smooth, radial function with compact support and $\int \eta \, dx = 1$. Let $\eta_\alpha(x) = \alpha^{-2}\eta(x/\alpha)$, which is an approximate identity. Let $\bar{\chi}_i$ be the characteristic function for Ω_i. Then $\sum_{i=1}^{N^2} \bar{\chi}_i = 1$ except on a set of measure zero. Let $\phi_i = \eta_\alpha * \Omega_i$. Then

$$\sum_{i=1}^{N^2} \phi_i(x) = \int \eta_\alpha(x - y) \sum_{i=1}^{N^2} \bar{\chi}_i(y) \, dy = 1.$$

The support conditions are satisfied by taking α small enough.

We define a function $\iota(t)$ to be a τ_C-periodic function on $[0, \tau_C)$ which is defined by $\iota(t) = i$ if $t \in [t \in (i-1)/N^2\tau_C, i/N^2\tau_C)$, $i = 1, \dots, N^2$.

We partition each Ω_i into identical squares of side-length h chosen so that $2^m h = \ell/4$ for some $m \in \mathbb{N}$. Taking the union of these partitions gives a partition of Ω into a grid with sidelength h. Note the dyadic relationship between scales ensures that $\tilde{\Omega}_i$ is also a union of h-length squares which we label S_j. For convenience let

$$\chi_i := \chi_{\tilde{\Omega}_i}$$

We define a time-dependent, local interpolant operator based on volume elements as follows:

$$I_{h,t} f := \chi_{\tilde{\Omega}_{\iota(t)}}(x) \sum_j \left(\chi_{S_j}(x) - \frac{h^2}{\sqrt{|\tilde{\Omega}_{\iota(t)}|}} \right) \frac{1}{h^2} \int_{S_j} f(y)\, dy.$$

Note that $I_{h,t}$ is supported on $\tilde{\Omega}_{\iota(t)}$. Additionally,

$$\|I_{h,t} f\|_{L^2} \leq C_I \|f \chi_{\tilde{\Omega}_{\iota(t)}}\|_{L^2}, \tag{3}$$

and

$$\|u \chi_{\tilde{\Omega}_{\iota(t)}} - I_{h,t}(u)\|_{L^2} \leq C_I h \|(\nabla u) \chi_{\tilde{\Omega}_{\iota(t)}}\|_{L^2}. \tag{4}$$

The proofs of these estimates are identical to those for the interpolant I_h. Note that the optimal constants in the above estimates are not the same but it is convenient to lump them together under the label C_I.

Note that the observation window spends τ_C/N^2 units of time in each of the regions Ω_i. Movement from one region to another is discontinuous. It should not be hard to adjust the analytic results in this paper to the case of continuous movement, although the conditions for data assimilation would change. The order that Ω_i are cycled through does not matter.

For each ϕ_i we denote a complimentary cut-off function by

$$\psi_i = \sum_{i \neq j} \phi_j, \tag{5}$$

so that $\psi_i + \phi_i \equiv 1$ on Ω. We say Ω_i is *dominant* if

$$\int |w|^2 \phi_i \, dx \geq \frac{1}{N^2} \int |w|^2 \, dx$$

and *active* if

$$\int |w|^2 \phi_i \, dx \geq \frac{1}{c_0 N^2} \int |w|^2 \, dx,$$

for some $c_0 > 1$. This parameter appears in the statement of Theorem 1.1 below—larger values of c_0 make the conditions in the theorem more stringent. Clearly, sine $\chi_i \geq \phi_i$, if Ω_i is active, then we also have

$$\int |w|^2 \chi_i \, dx \geq \frac{1}{c_0 N^2} \int |w|^2 \, dx.$$

Alternatively we say Ω_i^c is *codominant* if

$$\int |w|^2 \psi_i \, dx < \left(1 - \frac{1}{N^2}\right) \int |w|^2 \, dx$$

and *coactive* if

$$\int |w|^2 \psi_i \, dx < \left(1 - \frac{1}{c_0 N^2}\right) \int |w|^2 \, dx.$$

Plainly, Ω_i is dominant if and only if Ω_i^c is codominant and Ω_i is active if and only if Ω_i^c is coactive.

1.3. **Data assimilation.** Suppose that u solves the 2D Navier-Stokes equations, written in projected form,

$$u_t - \nu\Delta u + \mathbb{P}(u\cdot\nabla u) = f; \qquad \nabla\cdot u = 0, \tag{6}$$

where $\mathbb{P}$ is the Leray projection operator. It is classical—see, e.g., [10]—that for large enough times any solution u becomes bounded solely by quantities determined by ν and f. In particular, the estimates (11) stated below hold. Throughout this paper we take this to be true starting from time $t = 0$. Note that since we are on a periodic domain $\Delta\mathbb{P} = \mathbb{P}\Delta$. The nudged equation for u is

$$v_t - \nu\Delta v + \mathbb{P}(v\cdot\nabla v) = f - \mu\mathbb{P}I_{h,t}(v-u); \qquad \nabla\cdot v = 0. \tag{7}$$

For reasonable choices of u_0 and f, and certain conditions on h and μ, this system admits a unique global smooth solution—see Remark 2.1. The difference $w = u - v$ satisfies

$$w_t - \nu\Delta w - \mathbb{P}(w\cdot\nabla w - w\cdot\nabla u - u\cdot\nabla w) = -\mu\mathbb{P}I_{h,t}(w); \qquad \nabla\cdot v = 0. \tag{8}$$

In the above we will take f to be sufficiently regular. Any solution u is eventually controlled by the Grashof number. We assume that this control holds at all positive times, which can be achieved by initiating our problem at a sufficiently large time for u.

Theorem 1.1. *Let $f \in L^\infty(0,\infty;L^2)$ be divergence free and mean zero. Let u be a solution to (6) with forcing f. Let the Grashoff number be defined by*

$$G := \limsup_{t\to\infty} \frac{2}{\nu^2\lambda_1}\|f(t)\|_{L^2}.$$

Under these assumptions, (7) is well-posed with a unique strong solution. Let v be the solution to (7) for u and f with initial data identically zero. Let $c_* > 0$ and $c_0 > 1$ be given. If

$$\begin{aligned}
\mu &\geq \max\left\{\nu\lambda_1 G^2, c_0 N^2(4\lambda_1 C_L^4\nu G^2 + c_*)\right\},\\
h &\leq \min\left\{\frac{\nu\lambda_1^{1/2}}{4C_I\mu}, \sqrt{\frac{\nu}{2C_I^2\mu}}\right\},\\
\tau_C &\lesssim \frac{1}{\mu}e^{-2C_L^4(G^2+2)},
\end{aligned}$$

where the suppressed constant only depends on c_*, c_0, λ_1, ν, C_L, C_I, N, L and ϕ_1, then,

$$\|(u-v)(t)\|_{L^2}^2 \leq e^{C_L^4}\nu^2 G^2 e^{-c_* t/2}. \tag{9}$$

The suppressed constant in the constraint on τ_C can be extracted from (C5), (C6) and (C7) below.

Remark 1.2. As is well-known, data assimilation results resembling [3] imply the classical determining parameter theorems of [15, 16, 19, 20]. These state that if two solutions to (6) agree at a course resolution, then they converge to each other exponentially. In our case, Theorem 1.1 implies a local version of such results. More precisely, if u and $\tilde{u}$ are two solutions to (6) with the same forcing satisfying the assumptions for u and f in Theorem 1.1, then, provided

$$I_{h,t}(u-\tilde{u})(t) = 0,$$

for all $t > 0$, we have that $\|(u - \tilde{u})(t)\|_{L^2} \to 0$ exponentially as $t \to \infty$. The precise statement of such a corollary can be improved—e.g., by assuming $I_{h,t}(u-\tilde{u})(t) \to 0$ as $t \to \infty$—but this would require additional work which is redundant to the existing literature.

1.4. **Organization and discussion of the proof.** Global *a priori* estimates are worked out in Section 2. In Section 3, local estimates are obtained which show that, if a region is dominant at time t_1, then it remains active for a short period of time assuming the Dirichlet quotient is suitably bounded. In Section 4, we prove Theorem 1.1. The proof involves two cases. The first case holds when the Dirichlet quotient is suitably bounded, and so, due to the work in Section 3, at least one region is active for a short period of time. This becomes our cycling time. If the interpolant cycles through all regions fast enough, then it must be in an active region for a short time. For these times, nudging is strong enough to drive synchronization across the full cycle time. In the second scenario, the Dirichlet quotient is bounded below which ensure dissipation is strong enough to drive synchronization without using the data assimilation term. Numerical tests are included in Section 5.

2. Global *a priori* estimates.

In this section we establish *a priori* bounds for solutions to (7) and (8). For a solution u to (6), it is well known that, if u_0 is divergence free, mean zero and belongs to H^1, and f is divergence free, mean zero and belongs to $L^\infty(0,\infty;L^2)$, then there exists a unique solution u to (6) which has zero mean. This solution satisfies a number of properties. We make use of the following which are taken directly from [3]—proofs can be found in [10, 29, 27] among other references. For any time T we have

$$u \in C([0,T];H^1) \cap L^2(0,T;H^2); \quad \frac{du}{dt} \in L^2(0,T;L^2). \tag{10}$$

Additionally,

$$\|u\|_{L^2}^2 \le \nu^2 G^2; \qquad \|\nabla u\|_{L^2}^2 \le \nu^2 \lambda_1 G^2; \qquad \int_t^{t+T} \|\Delta u\|_{L^2}^2 \, ds \le (1 + T\nu\lambda_1)\nu\lambda_1 G^2. \tag{11}$$

We take these properties to hold from time $t = 0$.

Following the classical literature, *a priori* estimates are obtained from the Grönwall inequality (see, e.g., [27]) which states that

$$x(t) \le x(0)e^{G(t)} + \int_0^t e^{G(t)-G(s)} h(s)\, ds; \qquad G(t) = \int_0^t g(r)\, dr,$$

provided

$$\frac{dx}{dt} \le g(t)x + h(t).$$

If $g = a$ and $h = b$ are constant, then we have

$$x(t) \le \left(x_0 + \frac{b}{a}\right)e^{at} - \frac{b}{a}.$$

2.1. **Energy estimate for v.** For the solution v to (7), we have

$$\frac{1}{2}\frac{d}{dt}\|v\|_{L^2}^2 + \nu\|\nabla v\|_{L^2}^2 = \langle f + \mu I_{h,t}(u), v\rangle - \mu\langle I_{h,t}(v), v\rangle. \tag{12}$$

Using Young's inequalities and (3), we have

$$\begin{aligned}\langle f+\mu I_{h,t}(u),v\rangle &\leq \frac{1}{\nu\lambda_1}\|f+\mu I_{h,t}(u)\|_{L^2}^2+\frac{\nu\lambda_1}{4}\|v\|_{L^2}^2\\ &\leq \frac{2{C_I}^2}{\nu\lambda_1}(\|f\|_{L^2}^2+\mu^2\|u\|_{L^2}^2)+\frac{\nu\lambda_1}{4}\|v\|_{L^2}^2.\end{aligned} \tag{13}$$

On the other hand

$$\mu\langle I_{h,t}(v),v\rangle=\mu\langle I_{h,t}(v)-v\chi_{\iota(t)},v\rangle+\mu\int|v|^2\chi_{\iota(t)}\,dx.$$

The second term above has a good sign. By (4), the remaining part satisfies

$$\mu\langle I_{h,t}(v)-v\chi_{\iota(t)},v\rangle\leq C_I\mu h\|\nabla v\|_{L^2}\|v\|_{L^2}\leq C_I\mu h\lambda_1^{-1/2}\|\nabla v\|_{L^2}^2.$$

Provided,

$$C_I\mu h\lambda_1^{-1/2}\leq\frac{\nu}{4}, \tag{C1}$$

it follows that

$$\frac{d}{dt}\|v\|_{L^2}^2+\frac{\nu\lambda_1}{2}\|v\|_{L^2}^2+\frac{\nu}{8}\|\nabla v\|_{L^2}^2\leq\frac{4C_I^2}{\nu\lambda_1}(\|f\|_{L^2}^2+\mu^2\|u\|_{L^2}^2), \tag{14}$$

and, by Grönwall, we conclude

$$\|v(t)\|_{L^2}^2\leq e^{-\nu\lambda_1 t}\|v(0)\|_{L^2}^2+\frac{4C_I^2}{\nu\lambda_1}(\|f\|_{L^2}^2+\mu^2\|u\|_{L^2}^2)(1-e^{-\nu\lambda_1 t}).$$

If $v(0)=0$ then, using the uniform bound on $\|u\|_{L^2}$ in (11), we get

$$\|v(t)\|_{L^2}^2\leq 4C_I^2[\nu^2+(\mu/\lambda_1)^2]G^2.$$

Integrating (14) we also obtain the bound

$$\frac{\nu}{8}\int_0^T\|\nabla v\|_{L^2}^2\,ds\leq\|v_0\|_{L^2}^2+\frac{4C_I^2T}{\nu\lambda_1}(\|f\|_{L^2}^2+\mu^2\|u\|_{L^2}^2).$$

Remark 2.1. Note that the above estimates are strong enough to prove estimates, existence and uniqueness as in [3, Theorem 5]. For mean zero data and forcing, v will be mean zero. Since the proofs are identical to the existing literature, we omit the details.

2.2. **Energy estimate for w.** For the solution $w=u-v$ to (8), we have by Ladyzhenskaya's inequality (1) that

$$\int(w\cdot\nabla u)\cdot w\,dx\leq C_L^2\|w\|_{L^2}\|\nabla w\|_{L^2}\|\nabla u\|_{L^2}.$$

Hence,

$$\begin{aligned}&\frac{1}{2}\frac{d}{dt}\|w\|_{L^2}^2+\nu\|\nabla w\|_{L^2}^2\\ &=-\int(w\cdot\nabla u)\cdot w\,dx-\mu(I_{h,t}(w)-w\chi_{\iota(t)},w)-\mu\int|w|^2\chi_{\iota(t)}\,dx\\ &\leq\frac{C_L^4}{2\nu}\|\nabla u\|_{L^2}^2\|w\|_{L^2}^2+\frac{\nu}{2}\|\nabla w\|_{L^2}^2+C_I^2\mu h^2\|(\nabla w)\chi_{\iota(t)}\|_{L^2}^2\\ &\quad+\mu\int|w|^2\chi_{\iota(t)}\,dx-\mu\int|w|^2\chi_{\iota(t)}\,dx,\end{aligned}$$

where we used the property (4). Choosing

$$C_I^2 \mu h^2 \le \frac{\nu}{2}, \tag{C2}$$

and using (11), we have

$$\frac{d}{dt}\|w\|_{L^2}^2 \le \frac{C_L^4}{\nu}\|\nabla u\|_{L^2}^2\|w\|_{L^2}^2 \le C_L^4 \nu\lambda_1 G^2 \|w\|_{L^2}^2$$

It follows that for $t \ge t_0$

$$\|w(t)\|_{L^2}^2 \le \|w(t_0)\|_{L^2}^2 e^{C_L^4\nu\lambda_1 G^2(t-t_0)}. \tag{15}$$

2.3. **Enstrophy estimate.** For the enstrophy, by a standard cancellation in the nonlinearity in the periodic setting, see [3, (14)-(15)] as well as [3, p. 294],

$$\frac{1}{2}\frac{d}{dt}\|\nabla w\|_{L^2}^2 + \nu\|\Delta w\|_{L^2}^2 = -\int (w\cdot\nabla w)\cdot\Delta u\, dx - \mu(I_{h,t}(w), \Delta w).$$

We have by (1) and Poincaré's inequality that

$$\begin{aligned}
\left|\int (w\cdot\nabla w)\cdot\Delta u\, dx\right| &\le \|w\|_{L^4}\|\nabla w\|_{L^4}\|\Delta u\|_{L^2} \\
&\le C_L^2\|w\|_{L^2}^{1/2}\|\nabla w\|_{L^2}\|\Delta w\|_{L^2}^{1/2}\|\Delta u\|_{L^2} \\
&\le C_L^2\lambda_1^{-1/2}\|\nabla w\|_{L^2}\|\Delta w\|_{L^2}\|\Delta u\|_{L^2} \\
&\le \frac{\nu}{2}\|\Delta w\|_{L^2}^2 + \frac{C_L^4}{2\nu\lambda_1}\|\nabla w\|_{L^2}^2\|\Delta u\|_{L^2}^2.
\end{aligned}$$

Hence,

$$\begin{aligned}
\frac{1}{2}\frac{d}{dt}\|\nabla w\|_{L^2}^2 + \nu\|\Delta w\|_{L^2}^2 &\le \frac{\nu}{2}\|\Delta w\|_{L^2}^2 + \frac{C_L^4}{2\nu\lambda_1}\|\nabla w\|_{L^2}^2\|\Delta u\|_{L^2}^2 - \mu(I_{h,t}(w),\Delta w) \\
&\le \nu\|\Delta w\|_{L^2}^2 + \frac{C_L^4}{2\nu\lambda_1}\|\nabla w\|_{L^2}^2\|\Delta u\|_{L^2}^2 + \frac{\mu^2 {C_I}^2}{2\nu}\|w\|_{L^2}^2,
\end{aligned}$$

where we used (3) and Young's inequality. We then have by Grönwall that, for $t > t_0$,

$$\begin{aligned}
\|\nabla w(t)\|_{L^2}^2 &\le \|\nabla w(t_0)\|_{L^2}^2 e^{\frac{C_L^4}{\nu\lambda_1}\int_{t_0}^t \|\Delta u(s)\|_{L^2}^2\, ds} \\
&\quad + \frac{\mu^2 C_I^2}{\nu}\int_{t_0}^t e^{C_L^4(\nu\lambda_1)^{-1}\int_s^t \|\Delta u(r)\|_{L^2}^2\, dr}\|w(s)\|_{L^2}^2\, ds \\
&\le \|\nabla w(t_0)\|_{L^2}^2 e^{C_L^4 G^2(1+\nu\lambda_1(t-t_0))} \\
&\quad + \frac{\mu^2 C_I^2}{\nu}(t-t_0)\sup_{t_0<s<t}\|w(s)\|_{L^2}^2 e^{C_L^4 G^2(1+\nu\lambda_1(t-t_0))},
\end{aligned}$$

where we used (11). Using (15) and assuming that

$$t - t_0 \le \mu^{-1}, \tag{C3}$$

we obtain

$$\begin{aligned}
\|\nabla w\|_{L^2}^2(t) &\le \|\nabla w(t_0)\|_{L^2}^2 e^{C_L^4 G^2(1+\nu\lambda_1\mu^{-1})} \\
&\quad + \frac{\mu C_I^2}{\nu}\|w(t_0)\|_{L^2}^2 e^{C_L^4\nu\lambda_1 G^2\mu^{-1}} e^{C_L^4 G^2(1+\nu\lambda_1\mu^{-1})}.
\end{aligned} \tag{16}$$

If

$$\nu\lambda_1 G^2 \le \mu, \tag{C4}$$

then this simplifies to

$$\|\nabla w\|_{L^2}^2(t) \leq \|\nabla w(t_0)\|_{L^2}^2 e^{C_L^4(G^2+1)} + \frac{\mu C_I^2}{\nu}\|w(t_0)\|_{L^2}^2 e^{C_L^4(G^2+2)}. \tag{17}$$

2.4. **Lower bound for $\frac{d}{dt}\|w\|_{L^2}^2$.** We also require a lower bound for $\frac{d}{dt}\|w\|_{L^2}^2$. To obtain this note that

$$\begin{aligned}
\frac{1}{2}\frac{d}{dt}\|w\|_{L^2}^2 &\geq -\nu\|\nabla w\|_{L^2}^2 - \left|\int (w\cdot\nabla u)\cdot w\,dx\right| - \left|\mu\langle I_{h,t}(w), w\rangle\right| \\
&\geq -\nu\|\nabla w\|_{L^2}^2 - C_L^2\|w\|_{L^2}\|\nabla w\|_{L^2}\|\nabla u\|_{L^2} - \mu C_I\|w\|_{L^2}^2 \\
&\geq -\nu\|\nabla w\|_{L^2}^2 - \frac{C_L^4}{\nu}\|w\|_{L^2}^2\|\nabla u\|_{L^2}^2 - \nu\|\nabla w\|_{L^2}^2 - \mu C_I\|w\|_{L^2}^2 \\
&\geq -2\nu\|\nabla w\|_{L^2}^2 - \frac{C_L^4}{\nu}\|w\|_{L^2}^2\|\nabla u\|_{L^2}^2 - \mu C_I\|w\|_{L^2}^2.
\end{aligned}$$

Then, by (C4),

$$\begin{aligned}
\frac{d}{dt}\|w\|_{L^2}^2 &\geq -4\nu\|\nabla w\|_{L^2}^2 - 2C_L^4\nu\lambda_1 G^2\|w\|_{L^2}^2 - 2\mu C_I\|w\|_{L^2}^2 \\
&\geq -4\nu\|\nabla w\|_{L^2}^2 - \mu(2C_L^4 + 2C_I)\|w\|_{L^2}^2.
\end{aligned} \tag{18}$$

2.5. **Bound for the Dirichlet quotient.** The Dirichlet quotient $\mathcal{Q}$ is defined to be

$$\mathcal{Q}(t) := \frac{\|\nabla w\|_{L^2}^2}{\|w\|_{L^2}^2}.$$

We introduce two scenarios:

- Scenario 1: all t such that $\mathcal{Q}(t) \leq \mu/\nu$ and,
- Scenario 2: all t such that $\mathcal{Q}(t) > \mu/\nu$.

Lemma 2.2. *Let μ satisfy (C4) and h satisfy (C2). Assume that t_1 is a scenario 1 time. Let*

$$\tau_{\mathcal{Q}} = \frac{1}{2\mu}\big((8C_I^2 + 2C_L^4 + 2C_I)e^{C_L^4(G^2+1)}\big)^{-1}.$$

Then, for all $t \in [t_1, t_1 + \tau_{\mathcal{Q}}]$,

$$\mathcal{Q}(t) \leq 4C_I^2\frac{\mu}{\nu}e^{C_L^4(G^2+2)}.$$

Proof. We have from (17) that, for $t_2 - t_1 \leq \mu^{-1}$, which is exactly (C3), and assuming t_1 is a Scenario 1 time,

$$\|\nabla w\|_{L^2}^2(t_2) \leq 2\frac{\mu C_I^2}{\nu}\|w(t_1)\|_{L^2}^2 e^{C_L^4(G^2+2)}. \tag{19}$$

From the mean value theorem, (18), (C3) and (C4), we have

$$\begin{aligned}
&\|w(t_2)\|_{L^2}^2 - \|w(t_1)\|_{L^2}^2 \\
&\geq (t_2 - t_1)\inf_{t_1<t<t_2}\frac{d}{dt}\|w\|_{L^2}^2(t) \\
&\geq (t_2 - t_1)\inf_{t_1<t<t_2}(-4\nu\|\nabla w\|_{L^2}^2 - (2C_L^4 + 2C_I)\mu\|w\|_{L^2}^2). \\
&\geq -(t_2 - t_1)\mu\|w(t_1)\|_{L^2}^2\big(8C_I^2 e^{C_L^4(G^2+1)} + (2C_L^4 + 2C_I)e^{C_L^4\nu\lambda_1 G^2(t_2-t_1)}\big) \\
&\geq -(t_2 - t_1)\mu\|w(t_1)\|_{L^2}^2\big((8C_I^2 + 2C_L^4 + 2C_I)e^{C_L^4(G^2+1)}\big),
\end{aligned} \tag{20}$$

where we used (19) and (15). It follows that

$$\|w(t_2)\|_{L^2}^2 \geq \left(1-(t_2-t_1)\mu\big((8C_I^2+2C_L^4+2C_I)e^{C_L^4(G^2+1)}\big)\right)\|w(t_1)\|_{L^2}^2. \tag{21}$$

If

$$t_2-t_1 \leq \frac{1}{2\mu}\big((8C_I^2+2C_L^4+2C_I)e^{C_L^4(G^2+1)}\big)^{-1}, \tag{22}$$

then

$$\|w(t_2)\|_{L^2}^2 \geq \frac{1}{2}\|w(t_1)\|_{L^2}^2. \tag{23}$$

Note that (22) implies (C3). So, using (19) in the numerator and (23) in the denominator, the Dirichlet quotient $\mathcal{Q}(t_2)$ is bounded by

$$\mathcal{Q}(t_2) \leq 4\frac{\mu C_I^2}{\nu}e^{C_L^4(G^2+2)},$$

provided $t_2-t_1 \leq \tau_C$. □

3. **Local estimates and active regions.** We make use of the following *local energy equality*,

$$\frac{1}{2}\frac{d}{dt}\|w\psi^{1/2}\|_{L^2}^2 = \langle \nu\Delta w + \mathbb{P}(w\cdot\nabla w - u\cdot\nabla w - w\cdot\nabla u) - \mu\langle \mathbb{P}I_{h,t}(w), w\psi\rangle \tag{24}$$

where ψ is a smooth non-negative function with compact support. This is obtained from (7) by testing against $w\psi$. In this section we establish an upper bound for the left-hand side of (24). By taking $\psi=\psi_i$ as defined in (5), this will imply that if a region is dominant at a given time t_1, then it remains active at least for a period of time depending on the parameters of the problem and $\|w(t_1)\|_{L^2}$.

Lemma 3.1. *Assuming $u, w \in H^1$ and $\psi \in \{\psi_i\}_{i=1}^n$ where ψ_i are defined in (5), we have*

$$\langle \mathbb{P}(w\cdot\nabla w - u\cdot\nabla w - w\cdot\nabla u), w\psi\rangle \leq C_L^2(\|w\|_{L^2}+4\nu G)\|\nabla w\|_{L^2}^2.$$

Proof. By the boundedness of $\mathbb{P}$ in L^p for $1<p<\infty$, the term in question satisfies

$$\begin{aligned}
&\|w\cdot\nabla w + u\cdot\nabla w + w\cdot\nabla u\|_{L^{4/3}}\|w\|_{L^4}\\
&\leq \big(\|\nabla w\|_{L^2}\|w\|_{L^4} + \|\nabla w\|_{L^2}\|u\|_{L^4} + \|\nabla u\|_{L^2}\|w\|_{L^4}\big)C_L\|w\|_{L^2}^{1/2}\|\nabla w\|_{L^2}^{1/2}\\
&\leq C_L^2\|w\|_{L^2}\|\nabla w\|_{L^2}^2 + C_L^2\|w\|_{L^2}^{1/2}\|\nabla w\|_{L^2}^{3/2}\|u\|_{L^2}^{1/2}\|\nabla u\|_{L^2}^{1/2}\\
&\quad + C_L^2\|\nabla u\|_{L^2}\|w\|_{L^2}\|\nabla w\|_{L^2}\\
&\leq C_L^2\|w\|_{L^2}\|\nabla w\|_{L^2}^2 + C_L^2\lambda_1^{-1/4}\|\nabla w\|_{L^2}^2\|u\|_{L^2}^{1/2}\|\nabla u\|_{L^2}^{1/2} + C_L^2\lambda_1^{-1/2}\|\nabla u\|_{L^2}\|\nabla w\|_{L^2}^2\\
&\leq C_L^2\|w\|_{L^2}\|\nabla w\|_{L^2}^2 + C_L^2 2\nu G\|\nabla w\|_{L^2}^2 + C_L^2 2\nu G\|\nabla w\|_{L^2}^2\\
&\leq C_L^2(\|w\|_{L^2}+4\nu G)\|\nabla w\|_{L^2}^2.
\end{aligned}$$

□

We now obtain an estimate on the local rate of change of the energy.

Lemma 3.2. *Assume u solves (6), v solves (7) and $\psi \in \{\psi_i\}_{i=1}^n$ as defined in (5). Also assume that t_1 is a scenario 1 time. Then, for all times t in $(t_1, t_1+\tau_{\mathcal{Q}})$, and letting $M > 0$ satisfy $\sup_{t_1<t<t_1+\tau_{\mathcal{Q}}} \|w(t)\|_{L^2}^2 \leq M$, we have*

$$\begin{aligned}&\frac{d}{dt}\|w\psi^{1/2}\|_{L^2}^2\\ &\leq \left[c_\psi \frac{\nu}{2r^2} + \mu C_I + C_L^2 M^{1/2} 4\frac{\mu}{\nu} C_I^2 e^{C_L^4(G^2+2)} + 16G\mu C_I^2 e^{C_L^4(G^2+2)}\right]\|w\|_{L^2}^2.\end{aligned}$$

Proof. We seek an upper bound for $\frac{d}{dt}\|w\psi^{1/2}\|_{L^2}^2$ where $\psi \in \{\psi_i\}_{i=1}^N$ is fixed. Our starting point is the local energy equality (24). We have, after integrating by parts,

$$\int \Delta w w\psi \, dx = -\int |\nabla w|^2 \psi \, dx + \frac{1}{2}\int w^2 \Delta\psi \, dx.$$

The first term on the right-hand side has a good sign and is dropped. Plainly

$$\nu \int w^2 \Delta\psi \, dx \leq c_\psi \nu r^{-2} \|w\|_{L^2}^2.$$

We also have

$$\mu |\langle \mathbb{P} I_{h,t} w, w\psi\rangle| \leq \mu C_I \|w\|_{L^2}^2.$$

From these estimates and Lemma 3.1 we obtain

$$\begin{aligned}&\frac{d}{dt}\|w\psi^{1/2}\|_{L^2}^2\\ &\leq \left(c_\psi \frac{\nu}{2r^2} + \mu C_I\right)\|w\|_{L^2}^2 + C_L^2(\|w\|_{L^2} + 4\nu G)\|\nabla w\|_{L^2}^2\\ &\leq \left[c_\psi \frac{\nu}{2r^2} + \mu C_I + C_L^2(M^{1/2} + 4\nu G)\mathcal{Q}\right]\|w\|_{L^2}^2\\ &\leq \left[c_\psi \frac{\nu}{2r^2} + \mu C_I + 4C_L^2 M^{1/2}\frac{\mu}{\nu} C_I^2 e^{C_L^4(G^2+2)} + 16G\mu C_I^2 e^{C_L^4(G^2+2)}\right]\|w\|_{L^2}^2,\end{aligned}$$

where we used Lemma 2.2. □

We are now ready to state our main observation about dominant and active regions, namely that, starting at a scenario 1 time, a dominant region remains active for a short period of time τ_C which can be quantified.

Lemma 3.3. *Fix $c_0 > 1$. Let $\mu \geq 1$ satisfy (C4) and h satisfy (C2) and (C7) below. Assume that t_1 is a scenario 1 time. Assume also that, for some $M > 1$ we have*

$$\|w(t_1)\|_{L^2}^2 \leq M.$$

Take $\tau_C > 0$ to be the minimum of the upper bounds in (C5), (C6) and(C7) below (note that $\tau_C \sim \mu^{-1}$). If a region Ω_i is dominant at time t_1 then Ω_i is active for all times in $[t_1, t_1+\tau_C]$. It follows that

$$\int |w(t_2)|^2 \chi_i \, dx \geq \frac{1}{c_0 N^2}\|w\|_{L^2}^2(t_2).$$

Remark 3.4. Above τ_C depends on $M = M(t_1)$. In principle τ_C could collapse as time passes since (15) allows for the growth of the energy of w. In our application, we will iteratively show that the energy is decaying exponentially as t_1 grows. So, this dependence on the energy will not lead to $\tau_C \to 0$ when we iterate to extend our result to all times.

Proof. Assume t_1 is a scenario 1 time and without loss of generality take $\Omega_i = \Omega_1$ to be dominant at time t_1. From Lemma 2.2, we have that $\mathcal{Q}(t) \le 4C_I^2 \frac{\mu}{\nu} e^{C_L^4(G^2+2)}$ on $[t_1, t_1+\tau_{\mathcal{Q}}]$. Then, by the mean value theorem, (15) and Lemma 3.2, we have

$$\begin{aligned}
&\|w\psi_1^{1/2}\|_{L^2}^2(t_2) - \|w\psi_1^{1/2}\|_{L^2}^2(t_1) \le (t_2-t_1) \sup_{t_1<t<t_2} \frac{d}{dt}\|w\psi_1^{1/2}\|_{L^2}^2 \\
&\le (t_2-t_1)\left[c_\psi \frac{\nu}{2r^2} + \mu C_I + 4C_L^2 M^{1/2}\frac{\mu}{\nu} C_I^2 e^{C_L^4(G^2+2)} + 16G\mu C_I^2 e^{C_L^4(G^2+2)}\right] \sup_{t_1<t<t_2} \|w(t)\|_{L^2}^2 \\
&\le (t_2-t_1)\left[c_\psi \frac{\nu}{2r^2} + \mu C_I + 4C_L^2 M^{1/2}\frac{\mu}{\nu} C_I^2 e^{C_L^4(G^2+2)} + 16G\mu C_I^2 e^{C_L^4(G^2+2)}\right] e^{C_L^4 \nu \lambda_1 G^2 (t_2-t_1)} \\
&\quad \cdot \|w(t_1)\|_{L^2}^2 \\
&\le (t_2-t_1) \underbrace{\left[c_\psi \frac{\nu}{2r^2} + \mu C_I + 4C_L^2 M^{1/2}\frac{\mu}{\nu} C_I^2 e^{C_L^4(G^2+2)} + 16G\mu C_I^2 e^{C_L^4(G^2+2)}\right] e^{C_L^4}}_{=:\mu K} \\
&\quad \cdot \|w(t_1)\|_{L^2}^2,
\end{aligned} \tag{25}$$

where we assumed $t_2 - t_1 < \tau_C$ where

$$\tau_C \le \tau_{\mathcal{Q}}, \tag{C5}$$

as this implies $\tau_C \le \mu^{-1}$. We additionally require

$$\tau_C \le \frac{\gamma}{\mu K}\left(1 - \frac{1}{N^2}\right), \tag{C6}$$

where

$$\gamma = \gamma(N, c_0) := \frac{1}{2}\left(\frac{1 - (\sqrt{c_0}N)^{-2}}{1 - N^{-2}} - 1\right) > 0. \tag{26}$$

Then, since Ω_1^c is codominant at time t_1, we get from (25) that

$$\begin{aligned}
\|w\psi_1^{1/2}\|_{L^2}^2(t_2) &\le \|w\psi_1^{1/2}\|_{L^2}^2(t_1) + \gamma\left(1 - \frac{1}{N^2}\right)\|w(t_1)\|_{L^2}^2 \\
&\le (1+\gamma)\left(1 - \frac{1}{N^2}\right)\|w(t_1)\|_{L^2}^2.
\end{aligned}$$

Note that γ is chosen so that the above prefactor is the midpoint between $1 - N^{-2}$ and $1 - (\sqrt{c_0}N)^{-2}$. We next guarantee

$$(1+\gamma)\left(1 - \frac{1}{N^2}\right)\|w(t_1)\|_{L^2}^2 \le \left(1 - \frac{1}{c_0 N^2}\right)\|w(t_2)\|_{L^2}^2, \tag{27}$$

again by controlling τ_C. If $\|w(t_1)\|_{L^2}^2 \le \|w(t_2)\|_{L^2}^2$, then we are done by our choice of γ and τ_C does not need to be updated. Otherwise, noting that (21) and $t_2 - t_1 < \tau_C$ imply

$$\|w(t_1)\|_{L^2}^2 < \left(1 - \tau_C \mu (8C_I^2 + 2C_L^4 + 2C_I) e^{C_L^4(G^2+1)}\right)\|w(t_2)\|_{L^2}^2,$$

we see that (27) is met provided

$$(1+\gamma)\left(1 - \frac{1}{N^2}\right)\left(1 - \tau_C \mu (8C_I^2 + 2C_L^4 + 2C_I) e^{C_L^4(G^2+1)}\right)^{-1} \le \left(1 - \frac{1}{c_0 N^2}\right),$$

which, in turn, holds if

$$\tau_C \leq \frac{1}{\mu(8C_I^2 + 2C_L^4 + 2C_I)e^{C_L^4(G^2+1)}}\left(1 - \frac{(1+\gamma)(1-N^{-2})}{1-(\sqrt{c_0}N)^{-2}}\right). \tag{C7}$$

We therefore take τ_C to be the minimum of the quantities listed above.

We have thus shown

$$\|w\psi_1^{1/2}(t_2)\|_{L^2}^2 < \left(1 - \frac{1}{c_0N^2}\right)\|w(t_2)\|_{L^2}^2,$$

that is, Ω_1^c is coactive at time t_2. Using the fact that $\phi_1 + \psi_1 = 1$, we have

$$\|w\phi_1^{1/2}(t_2)\|_{L^2}^2 \geq \frac{1}{c_0N^2}\|w(t_2)\|_{L^2}^2,$$

and therefore Ω_1 is active at time t_2. □

4. Mobile data assimilation.

4.1. Short time synchronization.

We now show that the data assimilation equation synchronizes regardless of whether we are in scenario 1 or scenario 2.

Lemma 4.1. *Assume that t_1 is a scenario 1 time. Let $c_* > 0$ and $c_0 > 1$ be given. Then, choosing μ to satisfy (C4), (C8) and (C9), and h to satisfy (C1) and (C2), and letting τ_C be as in Lemma 3.3, it follows that*

$$\|w(t_1 + \tau_C)\|_{L^2}^2 \leq \|w(t_1)\|_{L^2}^2 e^{-c_*\tau_C}.$$

The idea behind this lemma is that, as the observability window cycles through all regions over the interval $[t_1, t_1 + \tau_C]$, it remains in an active interval for τ_C/N^2 units of time. When this is the case, synchronization is driven by the nudging term at an exponential rate. Over the remaining times, $\|w\|_{L^2}^2$ might grow, but not enough to overcome the convergence during synchronization.

Proof. Suppose that Ω_i is the dominant region at time t_1. Then, by Lemma 3.3, which requires μ satisfy (C2) and (C4) and h satisfies (C2), it is active on $[t_1, t_1+\tau_C]$ and, therefore,

$$\int |w|^2\chi_i\,dx \geq \frac{1}{c_0N^2}\int |w|^2\,dx.$$

There exists a strict and maximal subinterval I of $[t_1, t_1 + \tau_C]$ on which the interpolant operator localizes to Ω_i. We may decompose $[t_1, t_1 + \tau_C]$ into the three intervals $[t_1, t_2]$, $I = [t_2, t_3]$, and $[t_3, t_1 + \tau_C]$, where $t_1 \leq t_2 \leq t_3$. The first or last interval can be degenerate. Note that $t_3 - t_2 = \tau_C N^{-2}$. On I, since Ω_i is active, by the Poincaré inequality we have

$$\begin{aligned}
&\frac{1}{2}\frac{d}{dt}\|w\|_{L^2}^2 + \nu\|\nabla w\|_{L^2}^2 \\
&= -\int (w\cdot\nabla u)\cdot w\,dx - \mu(I_{h,t}(w) - w\chi_{\iota(t)}, w) - \mu\int |w|^2\chi_{\iota(t)}\,dx \\
&\leq C_L^2\|\nabla u\|_{L^2}\|w\|_{L^2}\|\nabla w\|_{L^2} + \mu C_I h\|w\|_{L^2}\|\nabla w\|_{L^2} - \frac{\mu}{c_0N^2}\int |w|^2\,dx \\
&\leq \frac{1}{\nu}C_L^4\|\nabla u\|_{L^2}^2\|w\|_{L^2}^2 + \frac{\nu}{2}\|\nabla w\|_{L^2}^2 - \frac{\mu}{c_0N^2}\int |w|^2\,dx,
\end{aligned} \tag{28}$$

where we are using (C1). Then

$$\frac{d}{dt}\|w\|_{L^2}^2 \le 2(4C_L^4\nu\lambda_1 G^2 - \frac{\mu}{c_0N^2})\|w\|_{L^2}^2$$
$$\le \frac{-\mu}{c_0N^2}\|w\|_{L^2}^2,$$

provided

$$4C_L^4\nu\lambda_1 G^2 \le \frac{\mu}{c_0N^2}. \tag{C8}$$

Hence for $t \in [t_2, t_3]$ we have

$$\|w(t)\|_{L^2}^2 \le \|w(t_2)\|_{L^2}^2 e^{-\frac{\mu}{c_0N^2}(t-t_2)}.$$

In particular,

$$\|w(t_3)\|_{L^2}^2 \le \|w(t_2)\|_{L^2}^2 e^{-\frac{\mu}{c_0N^2}\frac{\tau_C}{N^2}}.$$

On the other hand, using (15), for $t \in [t_i, t_{i+1}]$ where $i = 1, 3$ we have

$$\|w(t)\|_{L^2}^2 \le \|w(t_i)\|_{L^2}^2 e^{4C_L^4\nu\lambda_1 G^2(t-t_i)}.$$

Hence,

$$\begin{aligned}\|w(t_1+\tau_C)\|_{L^2}^2 &\le \|w(t_3)\|_{L^2}^2 e^{4C_L^4\nu\lambda_1 G^2(t_1+\tau_C-t_3)}\\ &\le \|w(t_2)\|_{L^2}^2 e^{4C_L^4\nu\lambda_1 G^2(t_1+t_C-t_i)-\frac{\mu}{c_0N^2}\frac{\tau_C}{N^2}}\\ &\le \|w(t_1)\|_{L^2}^2 e^{4C_L^4\nu\lambda_1 G^2(t_1+\tau_C-t_3+t_2-t_1)-\frac{\mu}{c_0N^2}\frac{\tau_C}{N^2}}\\ &\le \|w(t_1)\|_{L^2}^2 e^{\tau_C(4C_L^4\nu\lambda_1 G^2-\frac{\mu}{c_0N^4})}\end{aligned}$$

Provided

$$4C_L^4\nu\lambda_1 G^2 - \frac{\mu}{c_0N^4} \le -c_*, \tag{C9}$$

we have

$$\|w(t_1+\tau_C)\|_{L^2}^2 \le e^{-c_*\tau_C}\|w(t_1)\|_{L^2}^2.$$

□

Lemma 4.2. *Suppose that scenario 2 holds on $[t_1, t_2]$. Let $c_* > 0$ and $c_0 > 1$ be given. Then for all $t \in [t_1, t_2]$, assuming μ satisfies (C9), and h satisfies (C1) we have*

$$\|w(t)\|_{L^2}^2 \le \|w(t_1)\|_{L^2}^2 e^{-c_*(t-t_1)}.$$

Proof. From (28) and dropping the term with the good sign, we have

$$\frac{1}{2}\frac{d}{dt}\|w\|_{L^2}^2 + \nu\|\nabla w\|_{L^2}^2 \le \frac{1}{\nu}C_L^4\|\nabla u\|_{L^2}^2\|w\|_{L^2}^2 + \frac{\nu}{2}\|\nabla w\|_{L^2}^2. \tag{29}$$

It follows that

$$\frac{d}{dt}\|w\|_{L^2}^2 + \mu\|w\|_{L^2}^2 \le 4C_L^4\nu\lambda_1 G^2\|w\|_{L^2}^2.$$

The desired result follows if

$$4C_L^4\nu\lambda_1 G^2 - \mu \le -c_*,$$

which is implied by (C9). □

Note that in (29) we drop the nudging term. Thus, in this lemma we are using diffusion to drive synchronization.

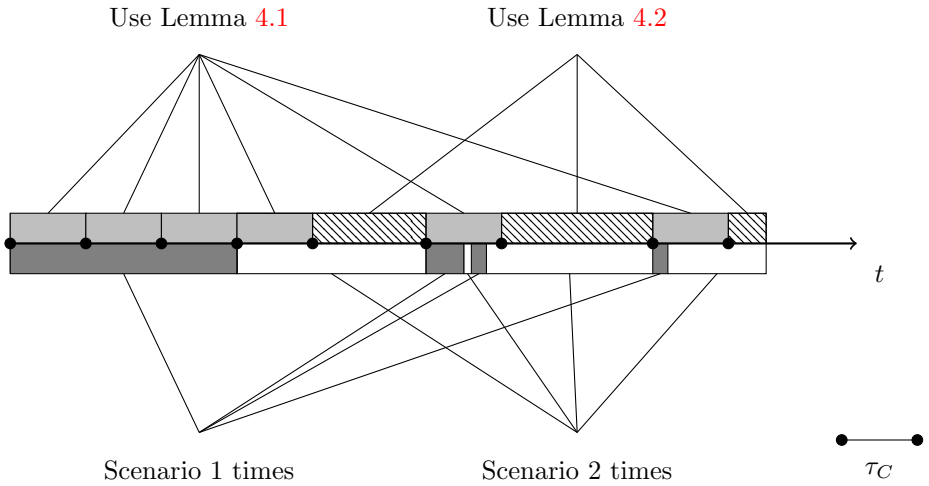

FIGURE 2. The partition scheme for the time axis in the proof of Theorem 1.1. The dark gray lower intervals represent scenario 1 times while scenario 2 times are unfilled. The gray upper intervals, which have length τ_C and are initiated at scenario 1 times, represent times across which at least one region stays active—see Lemma 3.3. On these intervals, nudging drives synchronization—see Lemma 4.1. In the hatched upper intervals, which can have any length, dissipation drives synchronization—see Lemma 4.2.

4.2. **Proof of Theorem 1.1.**

Proof. Let w be a solution to (7) on $\Omega \times (0,\infty)$ where $v_0 = 0$ so that $w_0 = u_0$. Suppose $t = t_0 = 0$ is a scenario 1 time—if it is not then, by Lemma 4.2, there is an interval originating at zero on which $\|w(t)\|_{L^2}^2$ is decreasing exponentially and we re-start this argument at the first scenario 1 time (if no time exists then Lemma 4.2 applies for all times and we are done). Let $I = [0, m\tau_C]$ where $m \geq 1$ is the largest integer such that, for all $i = 0, \dots, m-1$ we have $t = i\tau_C$ is a scenario 1 time. Note that $\|w(i\tau_C)\|_{L^2}$ is a decreasing sequence hence the parameters in Lemma 4.1, in particular τ_C, can be chosen uniformly depending on $M = \|u_0\|_{L^2}^2 \leq \nu^2 G^2$ (see Remark 3.4). Then

$$\|w(m\tau_C)\|_{L^2}^2 \leq e^{-c_* m\tau_C} \nu^2 G^2.$$

Additionally $m\tau_C$ is a scenario 2 time. Let t_1 be the first scenario 1 time after $m\tau_C$. So, by Lemma 4.2 we have for all $t \in [m\tau_C, t_1]$,

$$\|w(t)\|_{L^2}^2 \leq e^{-c_*(t-m\tau_C)} \|w(m\tau_C)\|_{L^2}^2 \leq e^{-c_*(t-m\tau_C)-c_* m\tau_C} \nu^2 G^2 = e^{-c_* t} \nu^2 G^2.$$

We can repeat this argument to generate a sequence of times t_i which grows without bound so that

$$\|w(t_i)\|_{L^2}^2 \leq e^{-c_* t_i} \nu^2 G^2.$$

This decay only holds on a sequence of times. We now extend this to decay for all times $t \geq \tau_C$. We can define a second sequence s_i so that $|s_{i+1} - s_i| \leq \tau_C$ and $\{t_i\} \subset \{s_i\}$, see Figure 4.2. This sequence also clearly satisfies $\|w(s_i)\|_{L^2}^2 \lesssim$

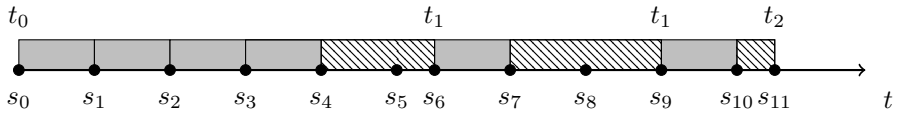

FIGURE 3. Refining the partition as in Figure 4.2. The new partition is segmented using the points labelled s_i. Note that $|s_{i+1} - s_i| \le \tau_C$.

$e^{-c_* s_i}\nu^2 G^2$. Then for $t \in (s_i, s_{i+1})$ we have by (15),

$$\begin{aligned}\|w(t)\|_{L^2}^2 &\le e^{C_L^4 \nu\lambda_1 G^2 (t-s_i)} \|w(s_i)\|_{L^2}^2 \\ &\le e^{C_L^4 \nu\lambda_1 G^2 \tau_C} \|w(s_i)\|_{L^2}^2 \\ &\le e^{C_L^4 \nu\lambda_1 G^2 \tau_C - c_* s_i} \nu^2 G^2.\end{aligned}$$

Note that for $\tau_C \le s_i$ we have $t/2 \le s_i$. So,

$$\|w(t)\|_{L^2}^2 \le e^{C_L^4 \nu\lambda_1 G^2 \tau_C - c_* t/2} \nu^2 G^2 \le e^{C_L^4} \nu^2 G^2 e^{-c_* t/2},$$

where we used the fact that $\tau_C \le \mu^{-1} \le (\nu\lambda_1 G^2)$ (which is (C4)).

The condition for μ in the theorem's statement is obtained from (C4) and (C9) while that for h is from (C1) and (C2). Presently, τ_C has been defined to be the smallest quantity in the right hand sides of (C5), (C6) and (C7). In the theorem's statement, however, we reduce this value for the sake of readability (it is still based on (C5), (C6) and (C7)). □

5. **Numerical tests.** Our tests are carried out on the NSE in vorticity form

$$\frac{d}{dt}\omega - \nu\Delta\omega + u \cdot \nabla\omega = g\,, \quad u = \nabla^\perp\psi, \quad -\Delta\psi = \omega \tag{30}$$

where $g = \nabla \times f$, the same time independent force concentrated on the annulus with wave numbers $10 \le |\mathbf{k}| < 12$, as used in [25, 26, 6]. While our analysis has been done in terms of velocity, we expect the nudging algorithm to work as well for vorticity. For the numerical results to follow, we simultaneously solve both (30) and the nudged equation as a coupled system

$$\frac{d}{dt}\tilde\omega - \nu\Delta\tilde\omega + \tilde u \cdot \nabla\tilde\omega = g - J_h(\tilde\omega - \omega);, \quad \tilde u = \nabla^\perp\tilde\psi, \quad -\Delta\tilde\psi = \tilde\omega \tag{31}$$

using a fully dealiased pseudospectral code with N=512 modes in each direction over the full physical domain $[0, 2\pi]^2$.

As in [6], for all mobile local nudging we use a spectrally filtered interpolating operator J_h. We first move from Fourier coefficients to nodal values via an FFT^{-1} applied to $\tilde\omega - \omega$. After restricting to the subdomain, we use data at only every 2^p-th node in each direction, so that $p = 1, 2, 3, 4$, corresponds to $h = \pi/128, \pi/64, \pi/32$ and $\pi/16$, respectively. A recursively averaged operator $\mathcal{K}_p$ depicted in Figure 4 is used the smoothen the result over the subdomain D. We then transform back so that

$$J_h(\tilde\omega - \omega) = \mathrm{FFT} \circ \mathcal{K}_p \circ \chi_D \circ \mathrm{FFT}^{-1}(\tilde\omega - \omega)\,.$$

The viscosity is fixed at $\nu = 10^{-4}$, and the force is scaled so that the (traditional) Grashof number is

$$\frac{\|f\|_{L^2}}{\nu^2 \lambda_1} = 10^6 \, .$$

This results in a chaotic reference solution, which after 25,000 time units starting from zero initial vorticity, is presumed to essentially be on the global attractor. The time stepper is the third-order Adams-Bashforth method in [25, 26] in which the linear term is handled exactly through an integrating factor. The step size is taken to be $\Delta t = 0.001$. The larger step $\Delta t = 0.01$ was found in [26] to be sufficient for computing the reference solution, but the new nudging schemes synchronize quickly if the flow is sampled on a finer time scale. The relaxation parameter is fixed at $\mu = 50$ and nudging takes place over a moving subdomain of size $\pi/2 \times \pi/2$.

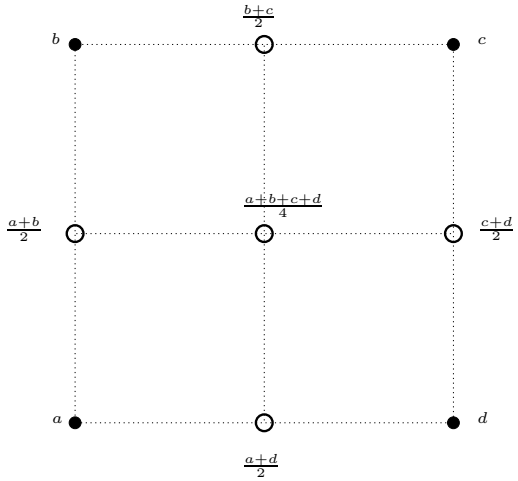

FIGURE 4. First recursive step of $\mathcal{K}_p$. Values of $\tilde{\omega}_N - \omega_N$ are a, b, c, d at the corners.

5.1. **Periodic movement of nudging subdomain.** We consider two cases in which the subdomain where the nudging takes place follows a regular pattern. The lower left corner of the subdomain is determined by functions $n_x(t)$, $n_y(t)$, that are periodic with period τ_C. In one scheme, these functions are similar to those in [6], and depicted for the case $\tau_C = 16$ in Figure 5 (Top). The second scheme simulates the situation covered by Theorem 1.1; the functions n_x, n_y are piecewise constant so that the subdomain moves in the same pattern as in Figure 5 (Bottom), but is held fixed for $\tau_C/16$ time units. In fact, due to the spatial discretization, both schemes use piecewise constant functions n_x, n_y. The difference is that the scheme using the functions in Figure 5 (Top) does so over a 512×512 grid in space, while the latter does so over a 4×4 spatial grid. Based on the functions in Figure 5 (Top), however, we will refer to the former as the *continuous scheme* and the latter as the *piecewise constant scheme*.

The results for the two regular pattern schemes are shown in Figure 6 for various cycling times. The relative L^2 errors are plotted top to bottom in the order corresponding to the legends. Both schemes eventually synchronize to within machine precision. In the case of continuous functions $n_x(t)$, $n_y(t)$, the rate of convergence

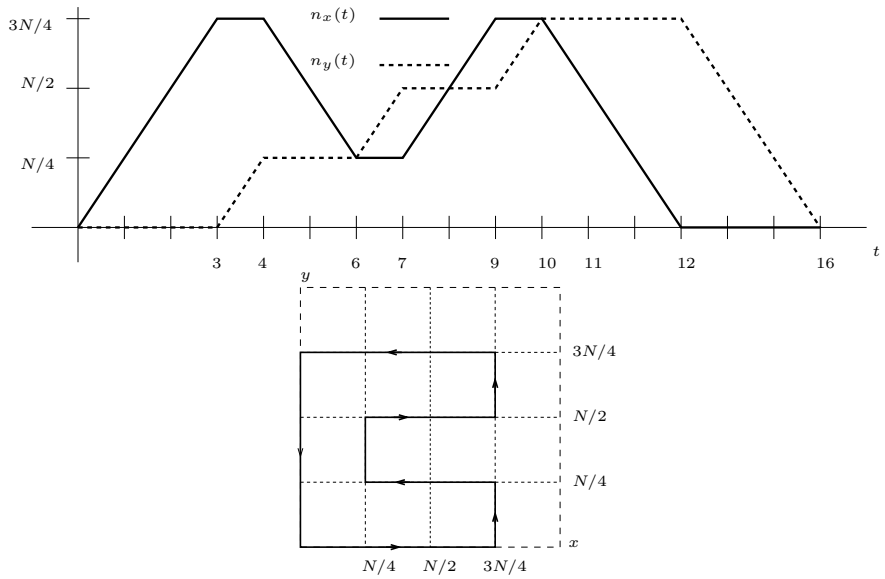

FIGURE 5. Movement of lower left corner of subdomain for patterned schemes.

improves as the cycling time increases over the range considered. In contrast, piecewise constant movement of the subdomain, the rates improve with faster cycling times, as suggested by the definition of τ_C.

The dependence on data resolution for both patterned movement schemes is shown in Figure 7. The continuous movement scheme appears to be somewhat more robust in that doubling the resolution of data did not slow the convergence as much as for the piecewise constant scheme. Finally, for both patterned schemes, we vary the relaxation parameter μ in Figure 8. For both schemes, the rate of convergence continues to improve with increasing μ through $\mu = 400$. If μ is too large (e.g. $\mu = 800$), the schemes are found to be unstable with time step $\Delta t = 0.001$.

5.2. **Nudging over the dominant subregion.** Motivated by the analysis in this paper, we also test an *informed scheme* which finds among the 16 subdomains in Figure 5 (Bottom) the most dominant one, nudges for a fixed period T over that subdomain, and repeats. The nudging on the subdomain is done using every other node in each direction, i.e., $p = 1$. The most dominant subdomain is determined by computing the trapezoidal rule approximation of the integral $\int_{\Omega_j} |\omega|^2$ for $j = 1, \ldots, 16$ on a coarse grid: using every 16^{th} node in each direction, i.e., $p = 4$. The (global) relative L^2 errors for this scheme are shown in Figure 9 (Top) for several values of T, done with $\mu = 50$. Comparing with Figure 8, we see that the best performance, achieved for $T = .02$, reaches machine precision just a bit faster than the two regular pattern schemes do using optimal values of μ. A zoom over the initial time range is shown in Figure 9 (Bottom), together with the ratios of $R_T = \int_{\Omega_j} |\omega|^2 / \int_{\Omega} |\omega|^2$ for $T = .04, .08$ and the line for the constant function $1/16$. As expected, the error drops the fastest when when this ratio is largest. As shown in Figure 10 (Top), unlike the two regular pattern schemes, the informed scheme seems to have a sweet spot for μ around 50. We note that the number of

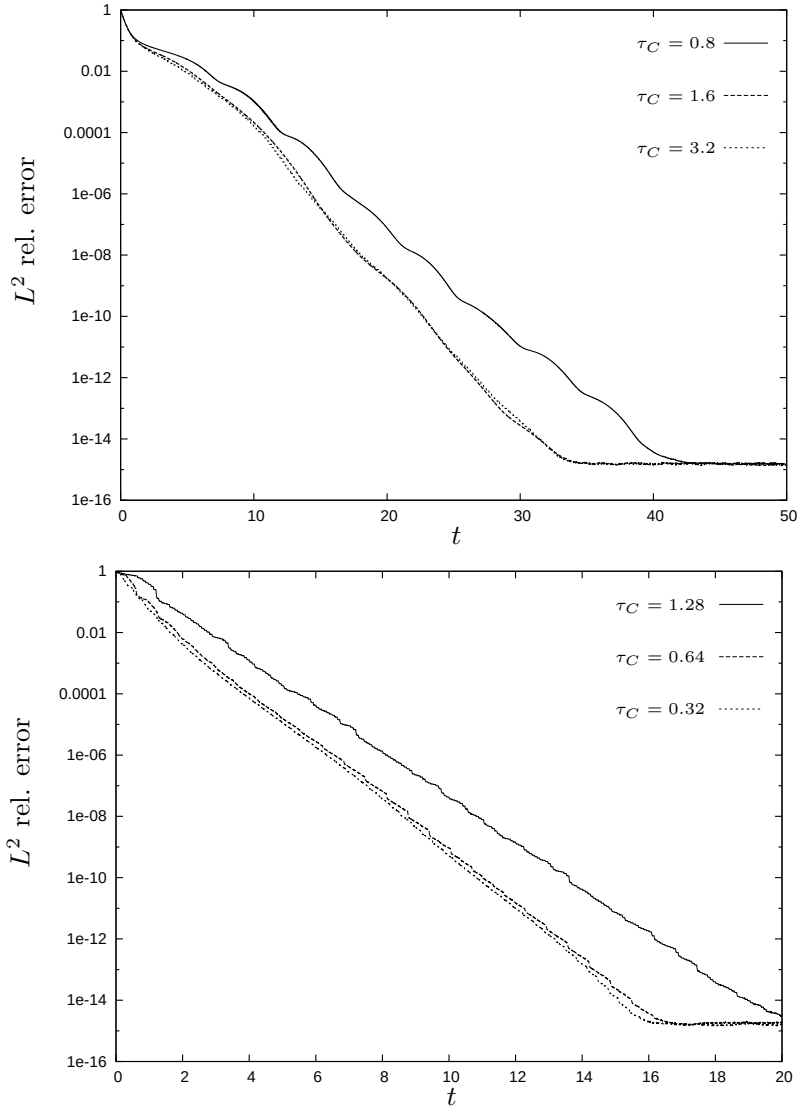

FIGURE 6. Dependence on cycling time. Top: continuous n_x, n_y. Bottom: piecewise constant n_x, n_y. For both, $\mu = 50$, $p = 1$.

observations, when using the nudging period $T = .02$, $p = 1$, and $\delta t = .001$, comes to $64^2 + 32^2/20 = 4147.2$ per step.

One can imagine a scenario where some time would be needed to move observational equipment from one subdomain to the next. We simulate this by introducing a delay at the moment the new dominant subdomain is determined. The delay is taken to be a significant fraction φ_{i} of the nudging period: in one case, one-fourth and in another, one-half. With the delay being at the beginning of that period, it is natural to expect a slowdown in synchronization, since the dominance of the subdomain fades. The results for these delays are shown in Figure 10 (Bottom) for the period $T = .02$. Also shown in Figure 10 (Bottom) is a plot for a scheme

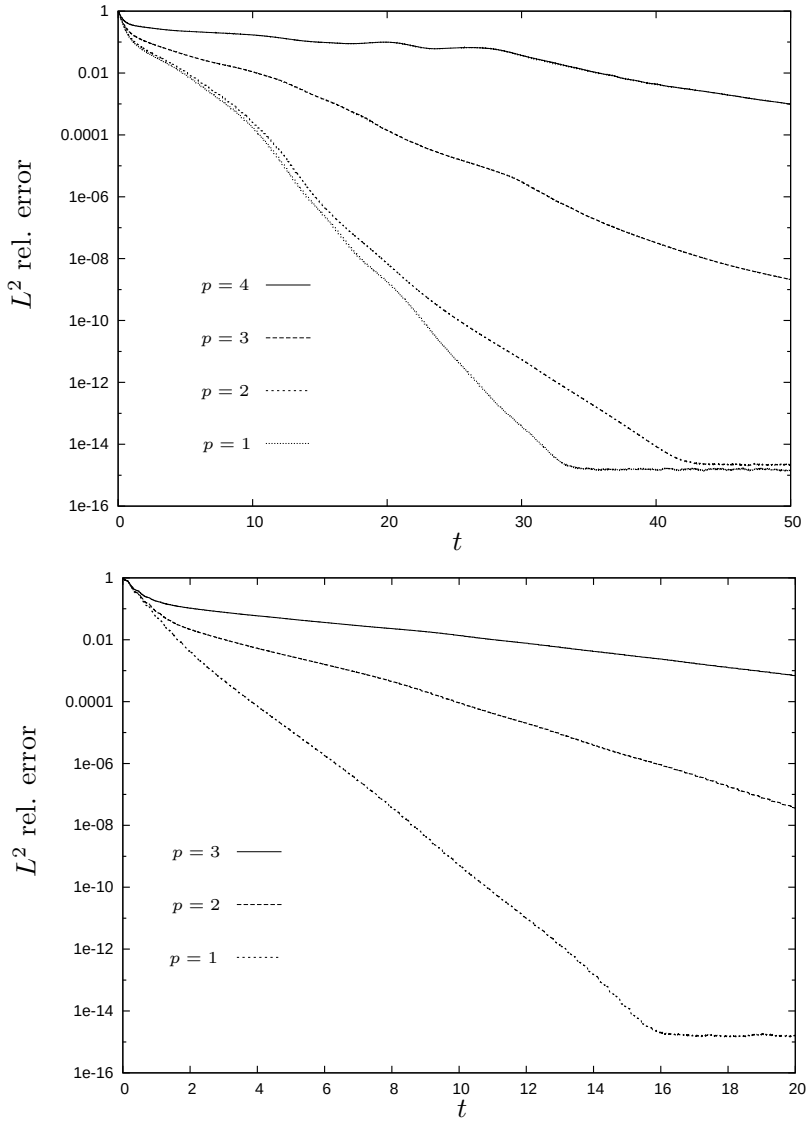

FIGURE 7. Dependence on data resolution. Top: continuous n_x, n_y, $\tau_C = 3.2$. Bottom: piecewise constant n_x, n_y, $\tau_C = 0.32$. For both $\mu = 50$.

where the next subdomain is chosen randomly, with no delay as well as with delay fractions $\varphi_{\mathrm{r}} = .25, .5$ of the nudging period. Such random movement is somewhat akin to the "bleeps" scheme in [17], except here the observers remain fixed and uniformly distributed over a subdomain for the nudging period, rather than moving freely throughout the full domain.

In our final test, we compare to purely spectral nudging. Recall that the data we have used to determine the dominating subregion corresponds, through an FFT, to the 32^2 lowest Fourier modes. Nudging at this global resolution can be simply affected by taking the interpolating operator to be projection onto those modes.

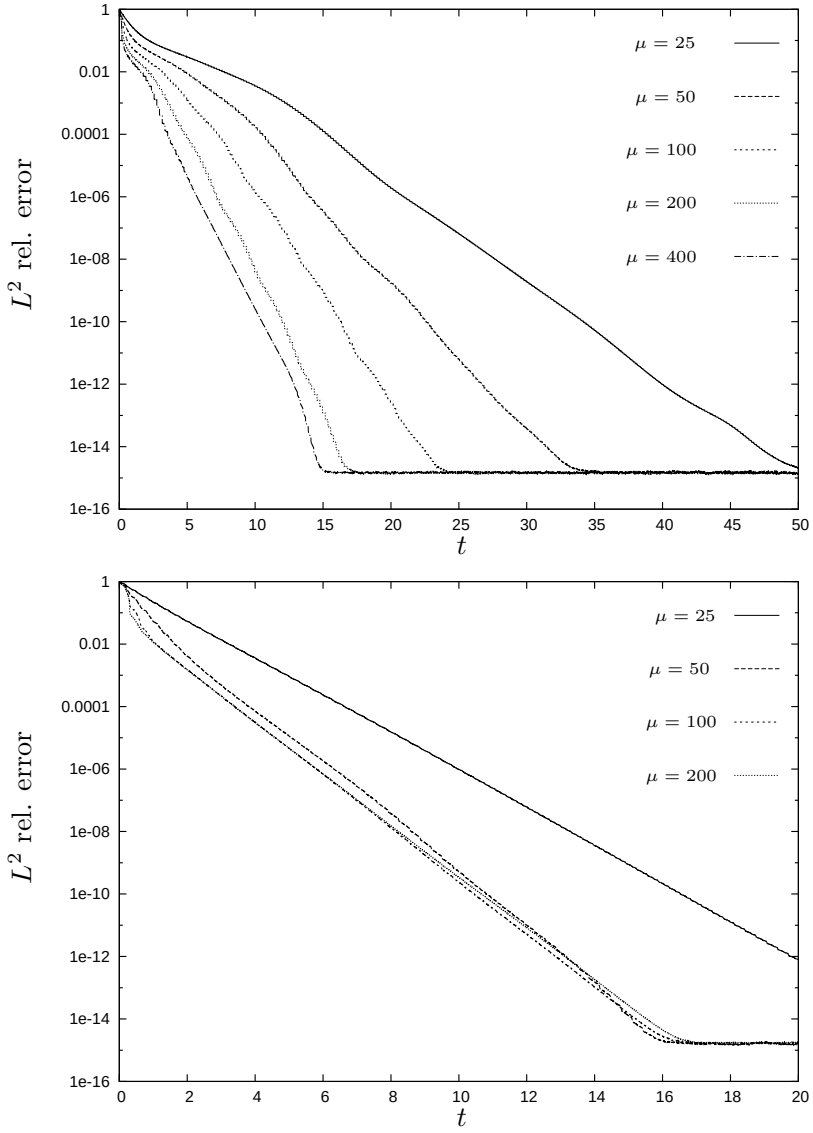

FIGURE 8. Dependence on μ. Top: continuous n_x, n_y, $\tau_C = 3.2$. Bottom: piecewise constant n_x, n_y, $\tau_C = 0.32$. For both $p = 1$.

We plot the result in Figure 11, together with that for the informed scheme for period $T = .02$ (no delay) and that for spectral nudging with $64^2 = 4096$ modes (nearly the amount of data, per time step, used for the informed scheme). We note that, initially, the error decreases faster for spectral nudging. To take advantage of this, we consider a hybrid scheme which uses spectral nudging with 32^2 modes until time $t = .1$ and then switches to the informed scheme. This results in faster synchronization to machine precision, though it used knowledge of an optimal time to switch. Such a hybrid scheme could be made practical by monitoring the error as Fourier projection is used and switching when a significant slowdown is detected.

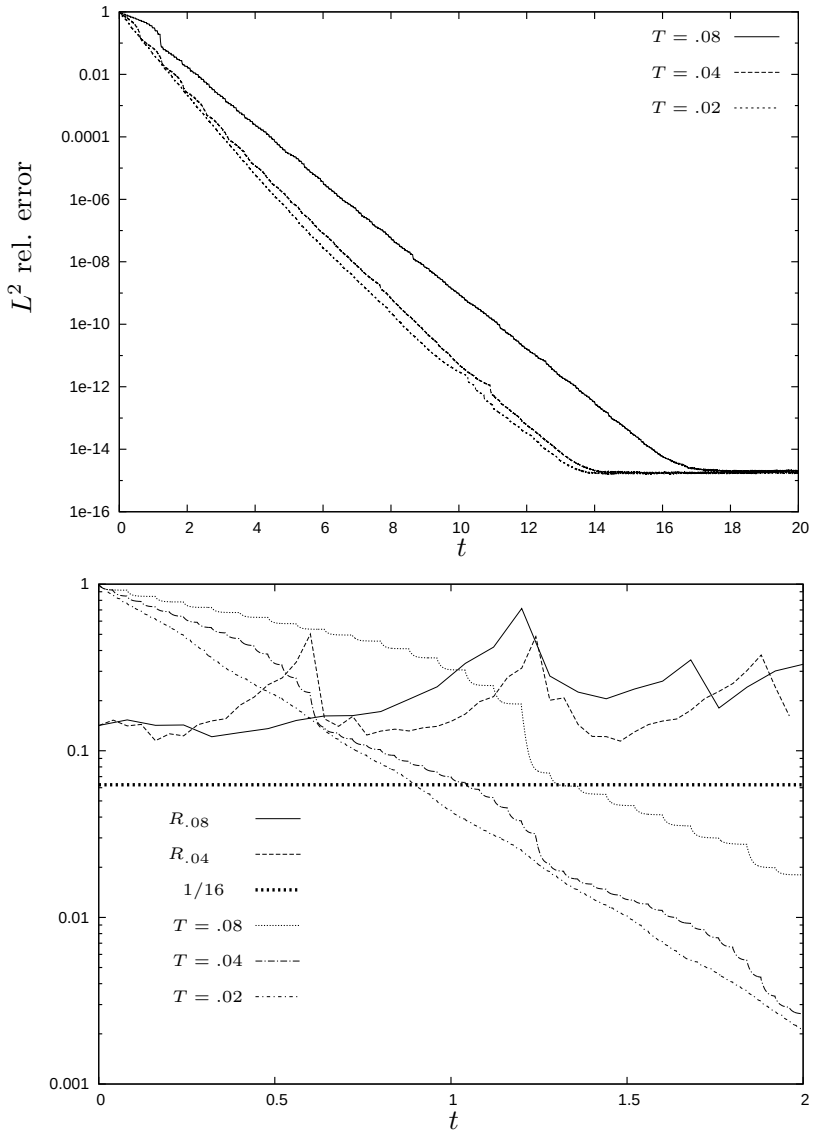

FIGURE 9. Top: effect of update period on informed scheme. Bottom: zoom of errors over initial time range along with their ratios R_T for $T = .04, .08$. For all, $p = 1$, $\mu = 50$.

5.3. **Summary of numerical results.** We have demonstrated that when the nudging subdomain moves in a regular pattern to cover the full domain, varying the speed of movement has a different effect depending on how smooth the movement is. For a scheme that faithfully simulates the assumptions in Theorem 1.1 faster movement results in faster synchronization. In contrast, for movement that is relatively smooth, the longer cycling times, over a certain range, gives faster synchronization. Smoother movement appears to be somewhat more robust with respect to coarsening the data resolution. After fine tuning the relaxation parameter

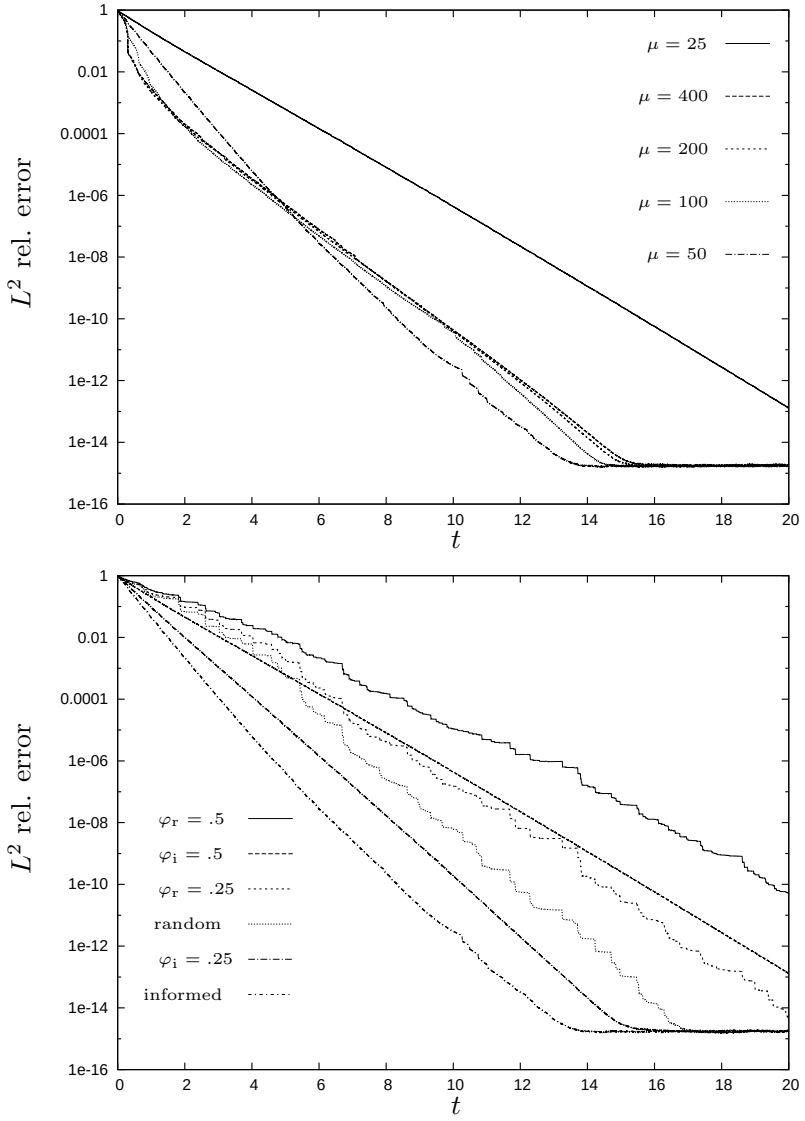

FIGURE 10. Top: dependence of informed scheme on μ, with $T = .02$, $p = 1$. Bottom: effect of delay in nudging, φ_i = delay fraction informed scheme, φ_r = delay fraction random scheme, $T = .02$, $\mu = 50$, $p = 1$ for both.

μ, synchronization to within machine precision is achieved after about 15 time units for the continuous scheme and about 16 units for the piecewise constant scheme. Nudging at that same resolution over the subdomain with the greatest L^2 error does so after about 13 time units. To be fair, this informed scheme requires an additional coarse mesh of observed data in order to determine the subdomain. This, however, is done only at the start of each nudging period. We have found a near optimal time period, over which to do the nudging before the determination of the next most dominant subdomain. This informed scheme synchronizes somewhat faster

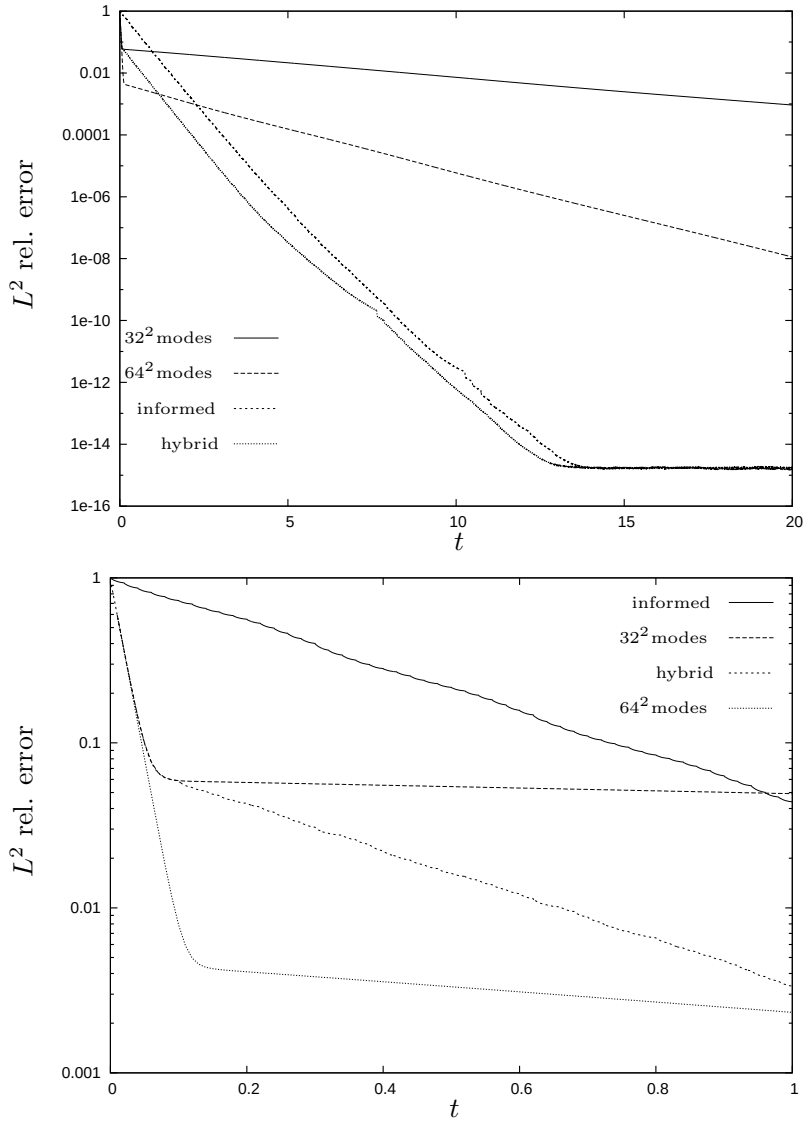

FIGURE 11. Comparing spectral nudging with informed scheme and a hybrid scheme, $T = .02$, switch at $t = .1$, both with $\mu = 50$.

than nudging for the same period with a subdomain that is randomly selected. In the case of the random scheme, over certain time intervals the error is nearly constant, punctuated by sharp drops when, presumably, the subdomain is dominant, or nearly so. These sharp declines are also to be expected since over the prior interval the error has held roughly steady, making the beneficial feedback stronger. Both the informed and random scheme appear to be robust against a significant delay before starting to nudge after each new subdomain is determined. Finally, we have found that while the informed scheme achieves much faster synchronization with a comparable number of data observations (per time step) than using global spectral nudging, the latter produces a sharper initial drop. We have demonstrated

the effectiveness of a simple hybrid scheme that switches from the spectral scheme to informed scheme, after this initial drop.

Acknowledgments. The second author is supported by [Simons Foundation via a Collaboration Grant (635438)]. All authors acknowledge the Lilly Endowment, Inc., through its support for the Indiana University Pervasive Technology Institute, which provided supercomputing resources [28]

REFERENCES

[1] D. A. F. Albanez, H. J. Nussenzveig Lopes and E. S. Titi, Continuous data assimilation for the three-dimensional Navier-Stokes-α model, *Asymptot. Anal.*, **97** (2016), 139-164.
[2] M. Asch, M. Bocquet and M. Nodet, *Data Assimilation: Methods, Algorithms, and Applications, Fundamentals of Algorithms*, 11. Society for Industrial and Applied Mathematics (SIAM), Philadelphia, PA, 2016.
[3] A. Azouani, E. Olson and E. S. Titi, Continuous data assimilation using general interpolant observables, *J. Nonlinear Sci.*, **24** (2014), 277-304.
[4] A. Azouani and E. S. Titi, Feedback control of nonlinear dissipative systems by finite determining parameters - a reaction diffusion paradigm, *Evol. Equ. Control Theory*, **3** (2014), 579-594.
[5] H. Bessaih, E. Olson and E. S. Titi, Continuous data assimilation with stochastically noisy data, *Nonlinearity*, **28** (2015), 729-753.
[6] A. Biswas, Z. Bradshaw and M. S. Jolly, Data assimilation for the Navier-Stokes equations using local observables, *SIAM J. Appl. Dyn. Syst.*, **20** (2021), 2174-2203.
[7] A. Biswas, C. Foias, C. F. Mondaini and E. S. Titi, Downscaling data assimilation algorithm with applications to statistical solutions of the Navier-Stokes equations, *Ann. Inst. H. Poincaré Anal. Non Linéaire*, **36** (2019), 295-326.
[8] A. Biswas and V. R. Martinez, Higher-order synchronization for a data assimilation algorithm for the 2D Navier-Stokes equations, *Nonlinear Anal. Real World Appl.*, **35** (2017), 132-157.
[9] E. Carlson, J. Hudson and A. Larios. Parameter recovery for the 2 dimensional Navier-Stokes equations via continuous data assimilation, *SIAM J. Sci. Comput.*, **42** (2020), A250-A270.
[10] P. Constantin and C. Foias, *Navier-Stokes Equations*, Chicago Lectures in Mathematics, University of Chicago Press, Chicago, IL, 1988.
[11] R. Daley, *Atmospheric Data Analysis*, Cambridge Atmospheric and Space Science Series, Cambridge University Press, Cambridge, 1991.
[12] A. Farhat, N. E. Glatt-Holtz, V. R. Martinez, S. A. McQuarrie and J. P. Whitehead, Data assimilation in large Prandtl Rayleigh-Bénard convection from thermal measurements, *SIAM J. Appl. Dyn. Syst.*, **19** (2020), 510-540.
[13] C. Foias, C. F. Mondaini and E. S. Titi, A discrete data assimilation scheme for the solutions of the two-dimensional Navier-Stokes equations and their statistics, *SIAM J. Appl. Dyn. Syst.*, **15** (2016), 2109-2142.
[14] C. Foias and G. Prodi, Sur le comportement global des solutions non-stationnaires des équations de Navier-Stokes en dimension 2, *Rend. Sem. Mat. Univ. Padova*, **39** (1967), 1-34.
[15] C. Foias and R. Temam, Determination of the solutions of the Navier-Stokes equations by a set of nodal values, *Math. Comp.*, **43** (1984), 117-133.
[16] C. Foias and E. S. Titi, Determining nodes, finite difference schemes and inertial manifolds, *Nonlinearity*, **4** (1991), 135-153.
[17] T. Franz, A. Larios and C. Victor, The Bleeps, the Sweeps, and the Creeps: Convergence Rates for Dynamic Observer Patterns via Data Assimilation for the 2D Navier-Stokes Equations, *Comput. Methods Appl. Mech. Engrg.*, **392** (2022), Paper No. 114673, 19 pp.
[18] J. Harlim and A. J. Majda, Catastrophic filter divergence in filtering nonlinear dissipative systems, *Commun. Math. Sci.*, **8** (2010), 27–43.
[19] D. A. Jones and E. S. Titi, Determining finite volume elements for the 2D Navier-Stokes equations. Experimental mathematics: Computational issues in nonlinear science (Los Alamos, NM, 1991), *Phys. D*, **60** (1992), 165-174.
[20] D. A. Jones and E. S. Titi, Upper bounds on the number of determining modes, nodes, and volume elements for the Navier-Stokes equations, *Indiana Univ. Math. J.*, **42** (1993), 875-887.

[21] E. Kalnay, *Atmospheric Modeling, Data Assimilation and Predictability*, Cambridge University Press, 2003.
[22] E. J. Kostelich, Y. Kuang, J. M. McDaniel, N. Z. Moore, N. L. Martirosyan and M. C. Preul, Accurate state estimation from uncertain data and models: An application of data assimilation to mathematical models of human brain tumors, *Biology Direct*, (2011).
[23] A. Larios and C. Victor, Continuous data assimilation with a moving cluster of data points for a reaction diffusion equation: A computational study, *Commun. Comp. Phys.*, **29** (2021), 1273-1298.
[24] P. A. Markowich, E. S. Titi and S. Trabelsi, Continuous data assimilation for the three-dimensional Brinkman-Forchheimer-extended Darcy model, *Nonlinearity*, **29** (2016), 1292-1328.
[25] E. Olson and E. S. Titi, Determining modes for continuous data assimilation in 2D turbulence, *J. Stat. Phys.*, **113** (2003), 799-840.
[26] E. Olson and E. S. Titi, Determining modes and Grashof number in 2D turbulence: A numerical study, *Theor. Comput. Fluid Dyn.*, **22** (2008), 327-339.
[27] J. C. Robinson, *Infinite-Dimensional Dynamical Systems. An Introduction to Dissipative Parabolic PDEs and the Theory of Global Attractors*, Cambridge Texts in Applied Mathematics, Cambridge University Press, Cambridge, 2001. xviii+461 pp. ISBN: 0-521-63204-8
[28] C. A. Stewart, V. Welch, B. Plale, G. Fox, M. Pierce and T. Sterling, Indiana university pervasive technology institute, Bloomington, In. https://doi.org/10.5967/K8G44NGB. (2017).
[29] R. Temam, *Navier-Stokes Equations. Theory and Numerical Analysis*, Reprint of the 1984 edition. AMS Chelsea Publishing, Providence, RI, 2001. xiv+408 pp. ISBN: 0-8218-2737-5.
[30] X. T. Tong, A. J. Majda and D. Kelly, Nonlinear stability of the ensemble Kalman filter with adaptive covariance inflation, *Commun. Math. Sci.*, **14** (2016), 1283-1313.
[31] X. T. Tong, A. J. Majda and D. Kelly, Nonlinear stability and ergodicity of ensemble based Kalman filters, *Nonlinearity*, **29** (2016), 657-691.

Received January 2023; revised May 2023; early access July 2023.